THE JOURNAL OF BIOLOGICAL CHEMISTRY
Vol. 278, No. 28, Issue of July 11, pp. 26174–26182, 2003
Printed in U.S.A.

Peptide Binding Induces Large Scale Changes in Inter-domain Mobility in Human Pin1*[S]

Received for publication, January 24, 2003, and in revised form, February 19, 2003
Published, JBC Papers in Press, April 9, 2003, DOI 10.1074/jbc.M300796200

Doris M. Jacobs‡§, Krishna Saxena‡, Martin Vogtherr‡, Pau Bernadó¶‖, Miquel Pons¶‖, and Klaus M. Fiebig‡

From the ‡Institut für Organische Chemie und Chemische Biologie, Johann Wolfgang Goethe-Universität Frankfurt, Marie-Curie Strasse 11, 60439 Frankfurt, Germany and the ¶Departament de Química Orgànica, Universitat de Barcelona, Martí I Franquès, 1-11, 08028 Barcelona, Spain

Pin1 is a peptidyl-prolyl *cis/trans* isomerase (PPIase) essential for cell cycle regulation. Pin1-catalyzed peptidyl-prolyl isomerization provides a key conformational switch to activate phosphorylation sites with the common phospho-Ser/Thr-Pro sequence motif. This motif is ubiquitously exploited in cellular response to a variety of signals. Pin1 is able to bind phospho-Ser/Thr-Pro-containing sequences at two different sites that compete for the same substrate. One binding site is located within the N-terminal WW domain, which is essential for protein targeting and localization. The other binding site is located in the C-terminal catalytic domain, which is structural homologous to the FK506-binding protein (FKBP) class of PPIases. A flexible linker of 12 residues connects the WW and catalytic domain. To characterize the structure and dynamics of full-length Pin1 in solution, high resolution NMR methods have been used to map the nature of interactions between the two domains of Pin1. In addition, the influence of target peptides on domain interactions has been investigated. The studies reveal a dynamic picture of the domain interactions. ^{15}N spin relaxation data, differential chemical shift mapping, and residual dipolar coupling data indicate that Pin1 can either behave as two independent domains connected by the flexible linker or as a single intact domain with some amount of hinge bending motion depending on the sequence of the bound peptide. The functional importance of the modulation of relative domain flexibility in light of the multitude of interaction partners of Pin1 is discussed.

Most peptidyl-prolyl *cis/trans* isomerases (PPIase)[1] play an important role during protein folding by catalyzing the *cis/trans* isomerization of peptidyl-prolyl imide bonds (1–4). Recently, with the discovery of the parvulin class of PPIases, peptidyl-prolyl isomerization has been identified as a key step in cell cycle regulation, oncogenesis, signal transduction, and a multitude of other cellular processes. Pin1 is the best-characterized PPIase of the parvulins and selectively catalyzes *cis/trans* isomerization of peptide sequences containing the phospho-Ser/Pro or phospho-Thr/Pro motif (pS/T-P) (5–7). Lu *et al.* (5) have proposed that, in the presence of certain kinases, Pin1 participates in a "tag and twist" mechanism to activate its substrate: the kinase phosphorylates the serine or threonine side chain (tagging), and Pin1 subsequently *cis/trans* isomerizes (twists) the peptide bond preceding proline in a di-peptide pS/T-P, thus introducing a marked kink in the backbone of the peptide chain.

Substrates of Pin1 include the mitotic regulators (Cdc25 phosphatase (8) and NIMA (9), PLK I, Wee, and Myt1 kinases); several transcription factors like β-catenin, c-Jun, and the tumor suppressor protein p53 (10–12); and some specific proteins like the RNA polymerase II, the cytoskeleton protein tau, and the G_1/S protein cyclin D1 (13, 14).

Pin1 is a two-domain protein of 18.4 kDa consisting of an N-terminal WW domain ($Pin1_{WW}$) important for substrate targeting (15), and a C-terminal catalytic domain ($Pin1_{CAT}$), which changes the substrate conformation by catalyzing the *cis/trans* isomerization of peptidyl-prolyl imide bonds. Previously reported x-ray and NMR structures of full-length Pin1 ($Pin1_{FL}$) reveal a global similarity of $Pin1_{CAT}$ with the FKBP-like class of PPIases and of $Pin1_{WW}$ with other WW domains found in single or tandem repeats in over 25 unrelated cell-signaling proteins (16).

Both domains selectively bind pS/T-P-containing substrate peptides, but only the catalytic domain isomerizes this sequence motif (7). Selectivity is achieved by specific phosphate-binding sites, of which one is located next to the active site of $Pin1_{CAT}$ and the other within the peptide binding epitope of $Pin1_{WW}$. Two x-ray studies and one NMR study have characterized the Pin1-peptide interactions previously: Ranganathan *et al.* (17) have solved the structure $Pin1_{FL}$ in complex with the Ala-Pro-dipeptide (PDB entry 1PIN), which is presumed to bind to the active site of the catalytic domain. Verdecia *et al.* (18) have elucidated the structure of $Pin1_{FL}$ complexed to the doubly phosphorylated peptide YpSPTpSPS of the C-terminal domain of the RNA polymerase II large subunit (PDB entry 1F8A). The NMR study of Wintjens *et al.* (19) compares the structure of free $Pin1_{WW}$ with $Pin1_{WW}$ in complex with peptides

* This work was supported in part by the LSF PARABIO. The costs of publication of this article were defrayed in part by the payment of page charges. This article must therefore be hereby marked "*advertisement*" in accordance with 18 U.S.C. Section 1734 solely to indicate this fact.

[S] The on-line version of this article (available at http://www.jbc.org) contains Supplemental Fig. S6 and Table SI.

§ To whom correspondence may be addressed. Tel.: 49-69-798-29740; Fax: 49-69-798-29741; E-mail: d.jacobs@nmr.uni-frankfurt.de.

‖ Supported by the Spanish Ministerio de Ciencia y Tecnologia (Grant BIO-2001-3115) and the Generalitat de Catalunya (CERBA).

** To whom correspondence may be addressed: Current address: Affinium Pharmaceuticals, 100 University Ave., 12th Floor North Tower, Toronto, Ontario M5J 1V6, Canada. Tel.: 416-645-6639; Fax: 416-646-1553; E-mail: kfiebig@afnm.com.

[1] The abbreviations used are: PPIase, peptidyl prolyl *cis/trans* isomerase; Cdc25, Pin1 binding peptide from the phosphatase Cdc25 (EQPLpTPVTDL-NH_2); CTD, Pin1 binding peptide from the C-terminal domain of the RNA polymerase II (YpSPTpSPS-NH_2); HSQC, heteronuclear single quantum coherence; NOE, nuclear Overhauser enhancement; $Pin1_{FL}$, full-length *h*Pin1; $Pin1_{CAT}$, catalytic domain of $Pin1_{FL}$; $Pin1_{WW}$, WW domain of $Pin1_{FL}$; Pintide, peptide WFYpSPR-NH_2; pS/T, phosphoserine/phosphothreonine; RDC, residual dipolar coupling; FKBP, FK506-binding protein; CPMG, Carr-Purcell-Meiboom-Gill.

from the Cdc25 phosphatase (Cdc25) and the cytoskeletal protein tau (PDB entries 1I6C, 1I8G, and 1I8H). Wintjens *et al.* suggest a unique binding scheme in which the peptide substrates all bind in the same orientation with the peptidyl-prolyl bond being in the trans conformation.

Pin1 encodes two functional elements, localization and catalysis, each in one separate domain. A flexible linker tethers both domains to one another. In terms of specificity toward proteins, it is functionally important to establish whether these domains are independent of one another or whether they interact in the absence and/or presence of the substrate. To address the impact of peptide binding on the inter-domain motion of the two domains of Pin1, we applied standard NMR methodology (20, 21). We have determined the domain-domain interaction surface of Pin1 under solution conditions by differential chemical shift mapping. Estimated overall correlation times derived from both ^{15}N spin relaxation data and HydroNMR calculations were analyzed to characterize the effects of peptide binding on the domain flexibility of $Pin1_{FL}$. Furthermore, residual dipolar couplings provided additional supporting information about domain-domain orientation and motion (22–25). In work now submitted for publication,[2] Brownian Dynamic simulations were performed to interpret the NMR relaxation properties of Pin1 with respect to global and inter-domain motion.

Full-length Pin1 ($Pin1_{FL}$) and the two domain fragments ($Pin1_{WW+L}$ and $Pin1_{L+CAT}$) have been studied in the presence of the following three different peptides: (i) the peptideWFYpSPR (Pintide), which was originally designed from a peptide library to be an optimal substrate for Pin1 (38); (ii) the doubly phosphorylated peptide YpSPTpSPS (CTD), which occurs as a heptad repeat in the C-terminal domain of the large subunit of RNA polymerase II; and (iii) the mono-phosphorylated peptide EQPLpTPVTDL (Cdc25), which is a model peptide from the essential mitotic phosphatase Cdc25 (1).

MATERIALS AND METHODS

Protein Production and Peptide Synthesis—Uniformly ^{15}N-labeled $Pin1_{WW+L}$, $Pin1_{L+CAT}$, and $Pin1_{FL}$ were expressed and purified as described previously (27). The protein samples contained 100 mM imidazole (pH 6.6), 100 mM NaCl, 5 mM dithioerythritol, 0.03% NaN_3, and 90% H_2O/10% D_2O.

All three phosphopeptides were synthesized according to literature procedures. Phosphorylated amino acids were purchased from Calbiochem-Novabiochem AG, Switzerland.

Binding Assays—The Pin1-peptide binding studies were conducted by monitoring changes in ^1H-^{15}N HSQC spectra. The chemical shift changes, Δ, were calculated using Equation 1.

$$\Delta_{1H+15N} = \sqrt{(\Delta_{1H})^2 + (0.17\Delta_{15N})^2} \quad \text{(Eq. 1)}$$

Generally, 0.25 mM protein solutions were employed. All three peptides were added in 8-fold excess.

To measure the dissociation binding constants (K_D) of Pintide and the CTD peptide binding to Pin1, HSQC spectra were recorded for a set of successively diluted samples with protein concentrations of 0.5, 0.2, 0.1, 0.05, and 0.02 mM. For these the protein-peptide ratio was fixed at 1:4, and the chemical shift changes due to the dissociation of the protein-peptide complex at successively lower protein (and peptide) concentrations were monitored. The observed chemical shift changes (Δ_{1H+15N}) were then fitted to the following expression by adjusting K_D and A,

$$\Delta_{1H+15N} = \frac{A}{2}\left\{5 + \frac{K_D}{P_0} - \sqrt{9 + \frac{10K_D}{P_0} + \left(\frac{K_D}{P_0}\right)^2}\right\} \quad \text{(Eq. 2)}$$

where P_0 is the total protein concentration, and $A = \delta_{free} - \delta_{bound}$, *i.e.* the difference in chemical shift between the free (δ_{free}) and bound (δ_{bound}) states. This equation has been derived from the mass law for the fixed protein-ligand ratio of 1:4 and results after substitution of Equation 4 into Equation 5 given in the literature (Ref. 26).

NMR Experiments and Data Analysis—All NMR experiments were recorded at 298 K on Bruker DRX800 and DRX600 spectrometers at 800- and 600-MHz proton resonance frequencies, respectively. Bruker *Xwinnmr3.1* software and *NMRView 5.0.4* (B. A. Johnson, Merck Research Laboratories) were used to process and analyze the data. All heteronuclear experiments were acquired with spectral widths of 31 ppm (F1) and 14 ppm (F2).

Backbone amide $\{^1H\}$-^{15}N NOE, ^{15}N R_1, ^{15}N R_2 (Carr-Purcell-Meiboom-Gill (CPMG)) values were measured at 600 MHz with conventional pulse sequences (28). The protein concentration was 0.5 mM. The CTD and Cdc25 peptides were added in 6-fold excess, whereas the concentration of Pintide was 2 mM due to its limited solubility. The ^{15}N R_1 and the ^{15}N R_2 relaxation decays were sampled at eight different time points each (T_1 delays = 0.005, 0.079, 0.079, 0.159, 0.239, 0.239, 0.359, 0.519, 0.759, and 1.119 s; T_2 delays = 0.009, 0.017, 0.017, 0.034, 0.060, 0.086, 0.086, 0.112, 0.148, and 0.190 s) with duplicate spectra for each time point. All spectra were acquired with 160 × 1024 complex points. A recycle delay of 4 s and eight transients were applied for the R_1 and R_2 experiments. For the unsaturated $\{^1H\}$-^{15}N NOE measurement, a recycle delay of 5 s was used. This recycle delay was substituted in the presaturated $\{^1H\}$-^{15}N NOE experiment with a 0.5-s delay followed by a 4.5-s long series of non-selective 120° ^1H pulses separated by 5-ms delay. The NOE spectra were recorded in an interleaved manner with 32 transients each.

Backbone amide ^{15}N R_1 and R_2 relaxation rates were determined by fitting peak heights as functions of relaxation decay times to single-exponential decay functions. Steady-state NOE values were calculated from the ratios of the peak intensities with and without proton saturation (29). The standard errors for R_1, R_2, and $\{^1H\}$-^{15}N NOE were estimated to 5%.

From a total of 156 backbone ^{15}N-amides, relaxation data were extracted for 118 residues of $Pin1_{FL}$, for 111 of Pintide-bound $Pin1_{WT}$, for 126 of CTD-bound $Pin1_{FL}$, and for 120 of Cdc25-bound $Pin1_{FL}$. For Pin_{WW+L} 46 out of 54 residues and for $Pin1_{L+CAT}$ 76 out of 109 residues were used for analysis. The residues Arg-17, Ser-18, Ser-19, Ser-42, Ser-43, Gly-44, Gln-75, Glu-76, and Glu-145 are not assigned. However, Ser-18 appears in the HSQC spectrum of peptide-bound $Pin1_{FL}$. 29 residues in $Pin1_{FL}$, 37 residues in Pintide-bound $Pin1_{FL}$, 22 residues in CTD-bound $Pin1_{FL}$, 28 in Cdc25-bound $Pin1_{FL}$, and 27 residues in $Pin1_{CAT}$ exhibit spectral overlap. The residues from which relaxation data were obtained and those used to determine the estimated overall correlation times are listed in the supplementary material. The isotropic correlation times were calculated using the program Tensor 2.0 (30). Two hundred Monte Carlo simulations were carried out to assess the validity of the isotropic diffusion model. Because the averaged correlation times are biased by the choice of residues, a range of correlation times was calculated resulting in deviations of 0.4 ns for $Pin1_{WW}$ and 0.1 ns for $Pin1_{CAT}$.

Because Pintide-bound $Pin1_{FL}$ is only saturated to ~85%, the relaxation rates are extrapolated to 100% saturation as follows,

$$R_{1,2}^{extr} = \frac{R_{1,2}^{obs} - (1 - \chi_{bound})R_{1,2}^{PinFL}}{\chi_{bound}} \quad \text{(Eq. 3)}$$

where $R_{1,2}^{extr}$, $R_{1,2}^{obs}$, and $R_{1,2}^{PinFL}$ are the R_1 and R_2 relaxation rates of saturated $Pin1_{FL}$-Pintide complex, the non-saturated $Pin1_{FL}$-Pintide complex, and the Apo-$Pin1_{FL}$, respectively, and χ_{bound} is the fraction bound or degree of saturation. The above extrapolation requires that bound and free peptide be in fast exchange, which can be safely assumed because we observe an averaging of the chemical shifts of the bound and free state in all titration studies used to determine the K_D values of the peptides.

Dipolar Couplings—We employed two types of media for the partially aligned media, a nonionic liquid crystalline medium and bacteriophages. The liquid crystalline medium (49) was prepared from 1-hexanol and C12E5 (Fluka). A 10% solution of this medium was prepared in buffer containing 10% D_2O. This solution was added in equal amounts to a 1 mM protein stock solution, yielding a final 5% medium/0.5 mM protein solution. For samples containing peptide, solid peptide was added until a solid precipitate emerged. Aligning samples containing phages (50) were prepared by adding a concentrated solution of filamentous phage PF11 (resulting concentration 21 mg/ml; Asla Ltd., Riga, Latvia) to the protein solution.

Alignment of the samples was monitored via the splitting of the deuterium signal. N-HN heteronuclear dipolar couplings of the sample containing phages were measured at 800 MHz using the IPAP scheme (31). N-HN heteronuclear dipolar couplings of the samples containing

[2] P. Bernadó, M. X. Fernandez, D. M. Jacobs, K. Fiebig, J. García de la Torre, and M. Pons, submitted for publication.

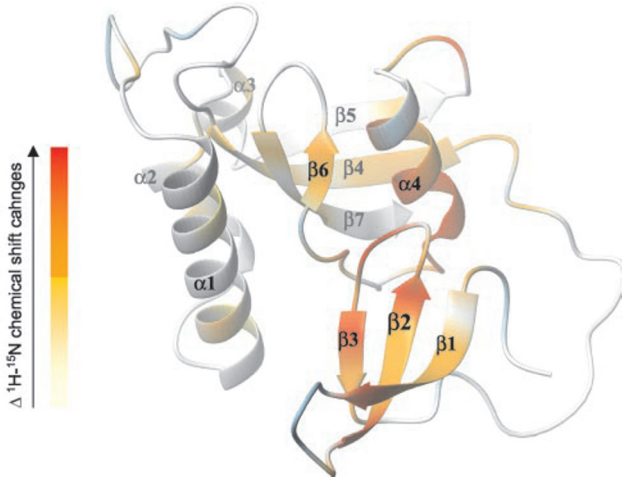

FIG. 1. **Mapping of the ^{1}H-^{15}N chemical shift differences between the isolated domains ($Pin1_{L+CAT}$ and $Pin1_{WW+L}$) and $Pin1_{FL}$ onto the x-ray structure of Ranganathan *et al.* (17).** *Different colors* encode the magnitude of the chemical shift changes: Δ_{1H+15N} = 0.005–0.01 (*yellow*); Δ_{1H+15N} = 0.01–0.025 (*orange*); Δ_{1H+15N} = 0.025–0.06 (*dark orange*); $\Delta_{1H+15N} > 0.06$ (*red*); unassigned residues and prolines (*light blue*). The most perturbed regions describe the hydrophobic cavity comprising the concave surface of the WW domain and the back side (strand β6 and helix α4) of the catalytic domain.

liquid crystalline medium were measured at 600 MHz as S^3E spectra (32). In each case, 256 T_1 data points were acquired and zero-filled to 1024 points. The splitting was evaluated using NMRView 5.0.4 (B. A. Johnson, Merck Research Laboratories). The RDC values were obtained by subtracting the reference value of the protein in isotropic solution.

Like for evaluation of relaxation data, the dipolar couplings were extrapolated to 100% saturation. The fraction bound was 85% for the phage solution and only 40% for the nonionic liquid crystals. The low saturation degree for the nonionic liquid crystals is due to peptide binding to the liquid crystals. Because the extrapolation of the data from the nonionic liquid crystals is less accurate, the data from phage solution were assumed to be more reliable. For analysis of the data we used Pales (33) and Module (34). In Pales, the tensor values were obtained using the SVD (35) and a maximum likelihood method (36). The Q value (21) was used to assess the agreement between experimental and theoretical values.

The x-ray structures of Apo-Pin1 (PDB entry 1PIN) and of Pin1 bound to the CTD peptide (PDB entry 1F8A) were used for all models; for consistency, we used the residue numbering of 1PIN for both structures. Protons were added to both structures. In all cases, the WW domain loop (residues Ser-16 to Arg-21) and the flexible linker (residues Glu-35 to Ala-53) have been omitted from the analysis. Coordinate files with an aligned arrangement of the two domain were generated semi-manually with Module (37).

RESULTS

The Two Domain Nature of Pin1 and the Role of the Flexible Linker—To characterize domain-domain interactions and dynamics NMR experiments were carried out on three different constructs of Pin1: (i) $Pin1_{FL}$, the full-length protein (residues 1–163); (ii) $Pin1_{WW+L}$, the isolated WW domain plus linker (residues 1–54); and (iii) $Pin1_{L+CAT}$, the isolated catalytic domain plus linker (residues 44–163). The residue numbering refers to that of the PDB structure 1PIN. Notably, each of the single-domain constructs includes the linker. Hence, the effect of the absence of a domain is studied rather than the absence of the covalently attached linker. This ensures minimal structural and chemical shift perturbation within the single domain constructs. All three constructs have been studied in the presence of three different peptides, namely WFYpSPR (Pintide), YpSPTpSPS (CTD), and EQPLpTPVTDL (Cdc25).

Differential Chemical Shift Mapping: Effect of the Linker—Fig. 1 shows the differences in chemical shifts between $Pin1_{FL}$ and either $Pin1_{L+CAT}$ or $Pin1_{WW+L}$, mapped onto the x-ray structure of Ranganathan *et al.* (17). As also seen in Fig. 2*A*, the strongest chemical shift perturbations due to the presence of the second domain are found in the β3 strand as well as the β1/β2 and β2/β3 loops of the WW domain forming the ends of its concave surface. In the catalytic domain, the chemical shift changes are clustered around the strand β6 and helix α4. Observed perturbations within strand β7 are likely due to the influence of the linker communicating the absence of the WW domain. Weaker shift perturbations are found for individual residues distributed throughout the catalytic domain. Interestingly, the most affected regions describe the hydrophobic cavity comprising the concave surface of the WW domain and the back side (strand β6 and helix α4) of the catalytic domain. Ranganathan *et al.* (17) have also identified this inter-domain interaction surface in their x-ray structure. However, in this study helix α1, which is only weakly perturbed in solution, is also included in the interaction surface. Notably, Pin1At, a homologous *cis/trans* isomerase from *Arabidopsis thaliana* lacking the WW domain, consists of negatively charged residues at the comparable surface (Pin1At: Asp-105, Asp-108, Glu-51, and Asp-52; *h*$Pin1_{FL}$: Gly-148, Phe-151, Gln-94, and Lys-95) (39). $Pin1_{WW}$ shields this surface of the catalytic domain. Hence, the two domains are most likely coupled by weak hydrophobic and hydrophilic inter-domain interactions and not directly by the linker, because this linker is too flexible to give rise to specific interactions. Interestingly, attractive forces between the domains are not large enough to persist without the linker. Mixing $Pin1_{WW+L}$ and $Pin1_{L+CAT}$, at 0.25 mM concentration, did not show any chemical shift perturbations when compared with the shifts of the individual domains. These studies clearly establish that WW and catalytic domains interact and that one role of the linker is to increase the local concentrations of each of the domains with respect to each other. The recently solved solution structure of Pin1 by Bayer *et al.* (40) confirms this weak interaction of both domains across the common binding interface, because no NOEs between the domains could be observed.

Effect of the Peptides—To study the interaction of three model peptides with $Pin1_{FL}$ and its isolated domains, it was necessary to know the saturation of the peptide-binding site located within the WW domain. In our studies the saturation of Pin1 with peptide was estimated to be 85% for Pintide (K_D = 200–400 μM), 90% for the CTD peptide (K_D = 200 μM), and 93% for the Cdc25 peptide (K_D = 117 μM (19)). The affinities determined in this study for Pintide and the CTD peptide are about one order of magnitude larger than the dissociation constants reported by Verdecia *et al.* (18), who found values of 17 μM for Pintide and 10 μM for the CTD peptide. The differences are likely due to the lower pH in our study (6.6 *versus* 7.5), which alters the protonation state of the phosphate group and thus affects binding (41, 42). Besides, increasing salt concentration decreases dramatically the PPIase activity of Pin1 implying that charges within or near the PPIase active site are also critical for a productive interaction between Pin1 with its substrate (42). Nevertheless the relative affinities for both peptides are reproduced as Pintide binds more strongly than the CTD peptide. Verdecia *et al.* (18) have reported that full-length Pin1 has higher apparent affinities to its substrates than its isolated domains. In Fig. 2 (*B–D*) chemical shift changes of three different peptides bound to each of the constructs ($Pin1_{FL}$, $Pin1_{L+CAT}$, or $Pin1_{WW+L}$) are shown as a function of residue number.

Peptide Binding to the Isolated Domains—The *yellow data points* in Fig. 2 show that all three peptides induce strong shift changes in $Pin1_{WW+L}$. Almost all residues within the WW domain are affected indicating that the peptide binding is as-

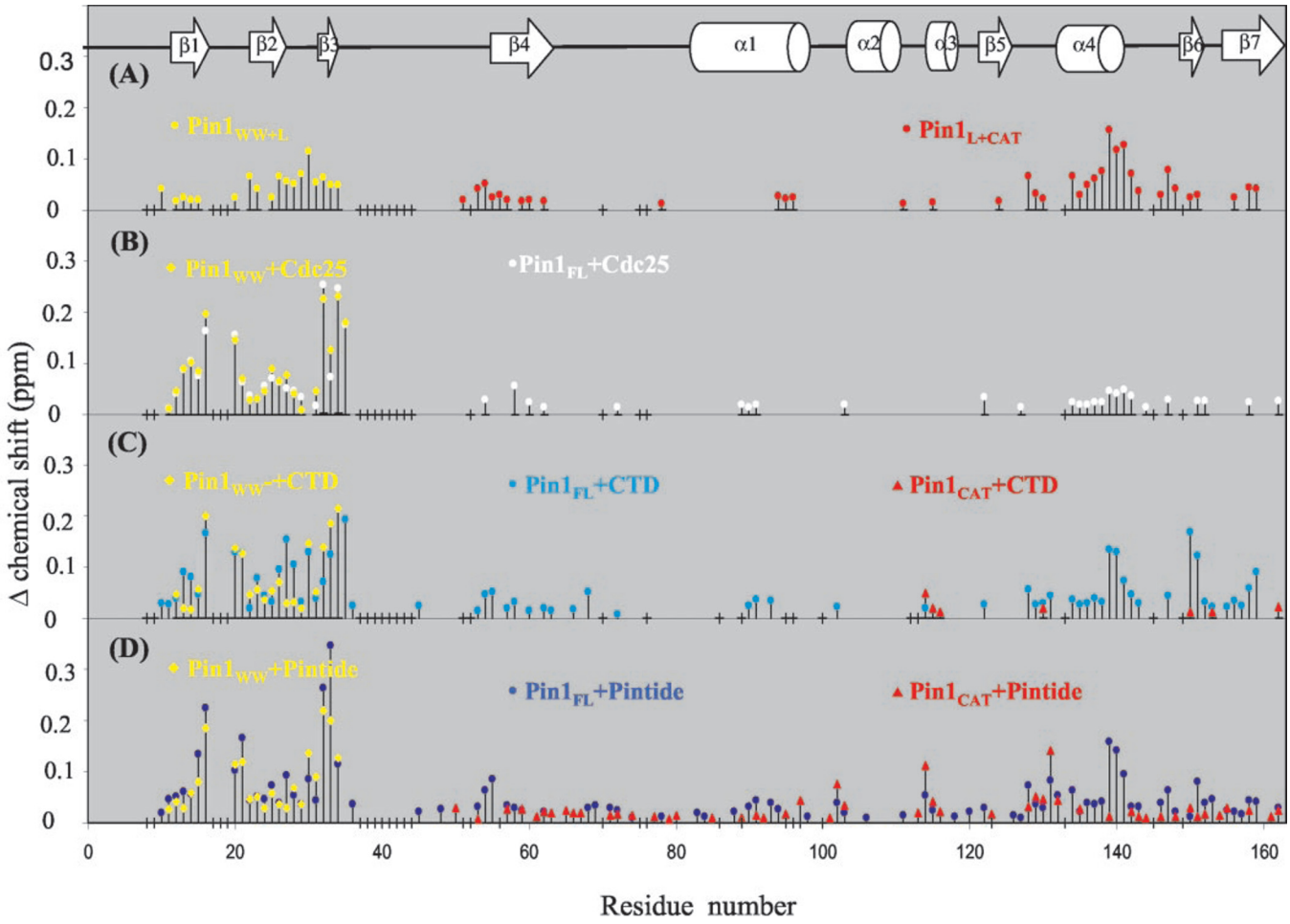

FIG. 2. *A*, 1H-15N chemical shift differences between Pin1FL and Pin1WW+L (*yellow*) and Pin1L+CAT (*red*). *B–D*, ^{1}H-^{15}N chemical shift changes between Apo-Pin1$_{FL}$ and Pin1$_{FL}$ complexed to EQPLpTPVTDL (Cdc25) (*white*), Apo-Pin1$_{FL}$ and Pin1$_{FL}$ complexed to YpSPTpSPS (CTD) (*cyan*), Apo-Pin1$_{FL}$ and Pin1$_{FL}$ complexed to WFYpSPR (Pintide) (*blue*); of Pin1$_{WW+L}$ and Pin1$_{WW+L}$ complexed to Pintide, CTD peptide, and Cdc25 peptide (*yellow*); and of Pin1$_{L+CAT}$ and Pin1$_{L+CAT}$ complexed to Pintide, CTD peptide, and Cdc25 peptide (*red*). *Vertical short bars* indicate unassigned residues.

sociated with conformational changes (19, 43). The pattern of chemical shift changes along the sequence is similar for all peptides supporting Wintjens' hypothesis (19) of conserved interactions between the WW domain and its various peptide substrates. In contrast, peptide binding to Pin1$_{L+CAT}$ is much more variable (*red data points* in Fig. 2): The Cdc25 peptide does not bind to the Pin1$_{L+CAT}$ construct at all, whereas Pintide provokes chemical shift changes spread over the entire catalytic domain. The CTD peptide only produces few shift changes localized mainly in helix α3.

Peptide Binding to Pin1$_{FL}$—As seen in Fig. 2 the amide chemical shift perturbations in Pin1$_{FL}$ upon binding each of the peptides are quite variable. Chemical shift perturbations within the WW domain are strong and affected by peptide binding to the small β-sheet, conformational changes of this β-sheet, and direct or indirect contacts with the catalytic domain. These effects are difficult to interpret. In comparison, the chemical shift perturbations observed in the catalytic domain are easier to interpret. In the case of Cdc25 binding to Pin1$_{FL}$, purely inter-domain effects cause the chemical shift changes, because this peptide does not bind to Pin1$_{L+CAT}$ at all. Domain-domain contacts are localized on the strand β6 and the helices α4 and α1 representing the hydrophobic surface of the back side of Pin1$_{CAT}$. Remarkably, this domain-domain interface is similarly perturbed when comparing chemical shift changes of Pin1$_{FL}$ with Pin1$_{L+CAT}$ suggesting that the Cdc25 peptide affects inter-domain interactions. Binding of the CTD peptide and Pintide to Pin1$_{FL}$ perturbs the same domain-domain interface. However, in these cases the effect of inter-domain interaction is overlaid with the effect of peptide binding to the PPIase site of the catalytic domain. In summary, the peptides rank by the number and strength of the observed chemical shift perturbations as Cdc25 < CTD < Pintide.

^{15}N NMR Relaxation—Heteronuclear relaxation measurements (R_1, R_2, and {^{1}H}-^{15}N NOE) (44) have been recorded for the isolated domains (Pin1$_{WW+L}$ and Pin1$_{L+CAT}$), for Apo-Pin1$_{FL}$ and for peptide bound Pin1$_{FL}$ (Pintide+Pin1$_{FL}$, CTD+Pin1$_{FL}$, and Cdc25+Pin1$_{FL}$) to analyze the relative mobility of the two domains. Generally, {^{1}H}-^{15}N NOE values of 0.824 (at 60 MHz) qualitatively reflect highly restricted internal motion, whereas values smaller than 0.65 are indicative of substantial internal motion. Negative values indicate completely disordered motion. Fig. 3*A* shows {^{1}H}-^{15}N NOE data revealing that for all cases the catalytic and the WW domains are well structured, whereas the linker is flexible in solution. Unlike the isolated SH3-SH2 fragment in the Src kinase whose linker residues are involved in nonspecific, hydrophobic domain-linker contacts and thus exhibit low positive {^{1}H}-^{15}N NOEs (20), the linker of Pin1$_{FL}$ is completely disordered. The flexibility of the linker is not notably reduced upon peptide binding. This suggests that the linker loosely connects the two domains but does not interact with the domains or the bound peptide. This is consistent with the fact that linker residues do not show electron density in the x-ray structures.

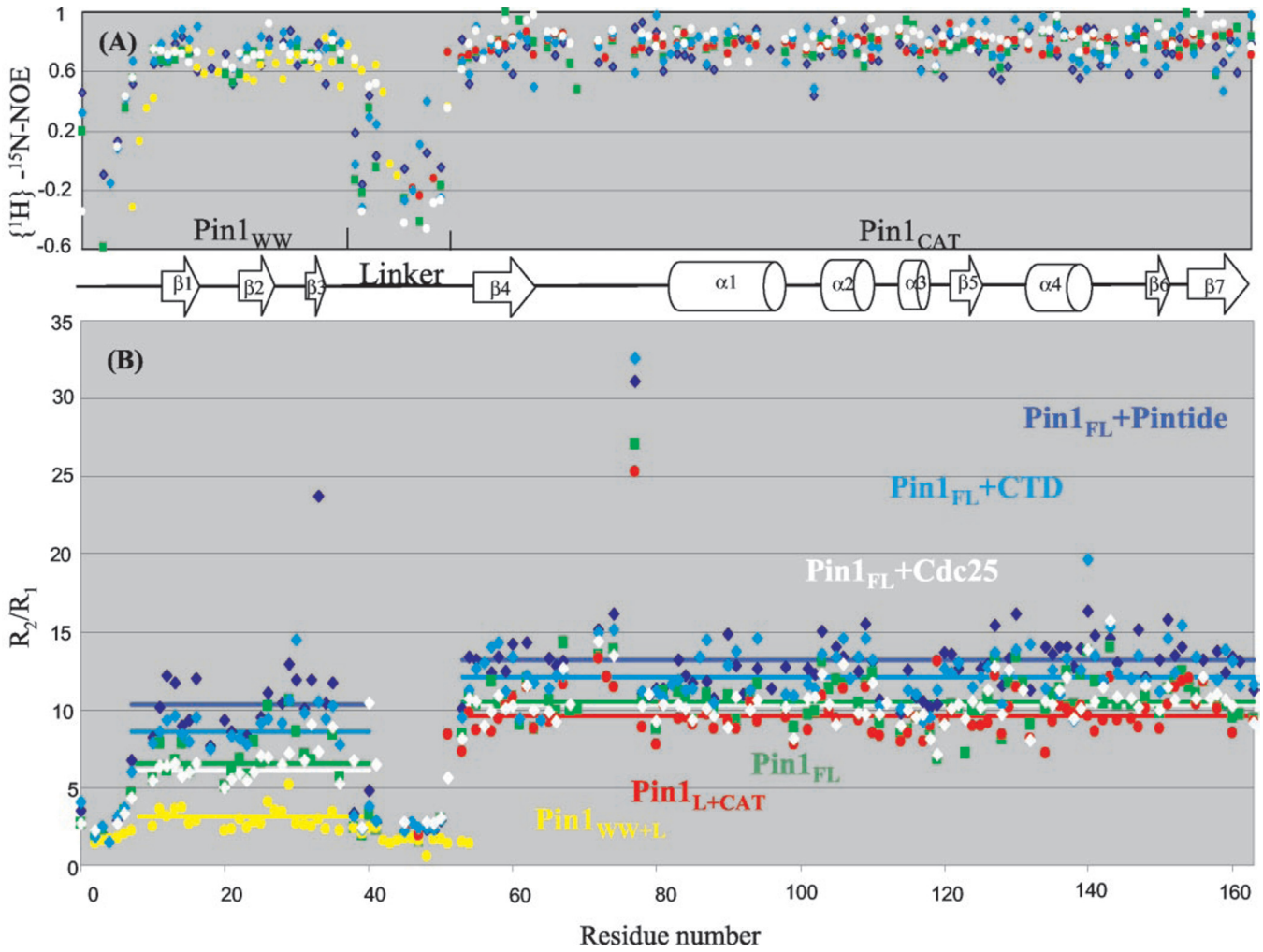

FIG. 3. **^{15}N relaxation data of Pin1$_{L+CAT}$ (*red*), Pin1$_{WW+L}$ (*yellow*), Pin1$_{WT}$ (*green*), Pin1$_{WT}$ complexed to Pintide (*blue*), Pin1$_{WT}$ complexed to CTD peptide (*cyan*), Pin1$_{WT}$ complexed to Cdc25 peptide (*white*).** *A*, the {^{1}H}-^{15}N NOE data show that the linker is flexible in solution, whereas the two domains are well structured. *B*, isotropic overall correlation times, t_c, were calculated from average R_2/R_1 values (*solid bars*) extracted from residues in secondary structure elements.

Backbone ^{15}N longitudinal and transverse relaxation rates, R_1 and R_2, are sensitive to rotational diffusive motion. To monitor inter-domain flexibility we estimate overall correlation times (τ_c) of the two domains in their free, linked, and complexed states from the R_2/R_1 ratio (Fig. 3*B*). In this approach, both internal and anisotropic motions are neglected. Only those residues in secondary structure elements without appreciable internal motion are taken into account. In addition, those residues are excluded that exhibit R_2/R_1 ratios that considerably deviate from the average value. This procedure still samples all possible orientations of the NH vectors in a reliable manner. The accuracy of the estimated τ_c depends on the number of selected residues, internal motion, and/or anisotropic motion. It is higher for Pin1$_{CAT}$ than for Pin1$_{WW}$, because significantly more residues could be selected in the larger catalytic domain and because Pin1$_{WW}$ is known to undergo significant conformational motion on the millisecond time scale (43). A summary of the estimated τ_c and a listing of residues they were derived from are given in Table SI (see Supplementary Material).

For further analysis of the estimated τ_c the following rigid sphere model depicted in Fig. 4 is assumed. Pin1 is thought to consist of two rigid spheres of different sizes connected by a flexible linker. The model assumes further that the domains tumble isotropically as rigid bodies. In this case, ^{15}N relaxation rates R_1 and R_2 are only a function of the overall τ_c, which is correlated with the volume via the Stokes-Einstein-Debye law and hence is proportional to the molecular weight of the domains. The model defines two limiting cases where (i) the two domains tumble independently of one another with correlation times τ_c^{WW+L} and τ_c^{L+CAT} and (ii) the domains stick together and tumble as one intact moiety with a $\tau_c^{FL\text{-}rigid}$ for the full-length rigid Pin1. According to the model, these limiting τ_c values are proportional to the masses of the constructs (m^{WW} = 4.51 kDa; m^{WW+L} = 5.55 kDa; m^{CAT} = 12.71 kDa; m^{L+CAT} = 13.75 kDa; and m^{FL} = 18.26 kDa). Any deviation from these extreme cases is described by an inter-domain interaction parameter x, which quantifies in a simple additive manner how much the τ_c of one domain will depend on the τ_c of the other domain as follows: $\tau_c^{WW}(x) = \tau_c^{WW+L} + x\tau_c^{CAT}$ and $\tau_c^{CAT}(x) = \tau_c^{L+CAT} + x\tau_c^{WW}$ (with $0 < x < 1$ and τ_c^{WW} and τ_c^{CAT} proportional to the molecular weights of the respective domains without the linker). The y-axis intercepts of these equations reflect the fact that a given domain will always interact with the entire linker, whose function is to increase the local concentration of the two domains. Each domain also interacts directly with the other domain via the domain-domain interaction surface as is described by the second term involving the x parameter. Fig. 4 depicts these theoretical curves and shows how well the experimental data fit to a model where the only adjustable parameter, $\tau_c^{FL\text{-}rigid}$, is chosen to be 11.6 ns to yield a residual R_2 value of 0.95.

We find that the experimental τ_c values of the isolated do-

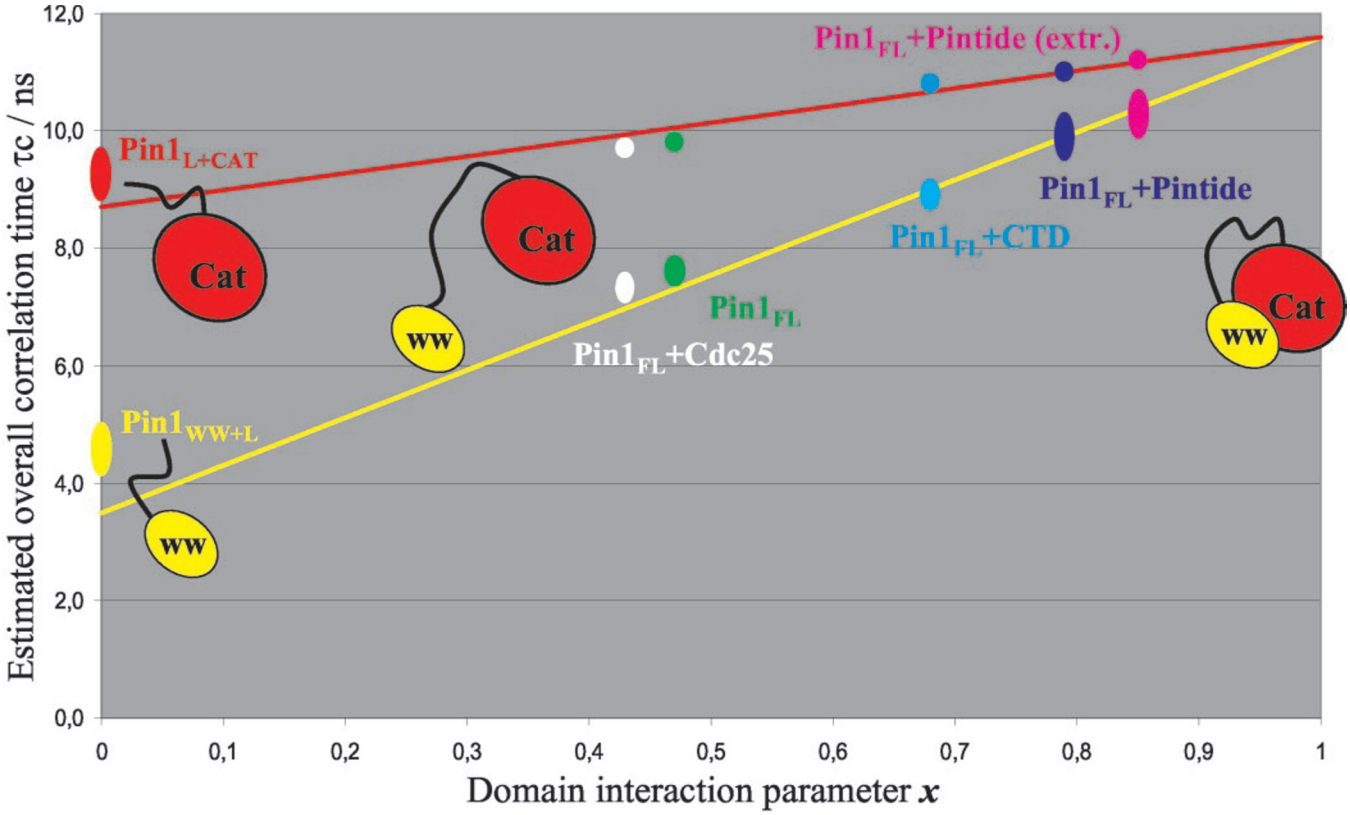

FIG. 4. **Estimated overall correlation times of $Pin1_{WW}$ (τ_c^{WW}) and of $Pin1_{CAT}$ (τ_c^{CAT}) when these domains are part of the full-length Pin1 as a function of the inter-domain interaction parameter *x* (see text for detail).** *Yellow* and *red lines* indicate the theoretical curves for the $Pin1_{WW}$ or $Pin1_{CAT}$, respectively. *Colored oval dots* represent experimental values and their uncertainties. $Pin1_{L+Cat}$ (*red*), $Pin1_{WW+L}$ (*yellow*), $Pin1_{FL}$ (*green*), $Pin1_{FL}$ complexed to Pintide (*blue*), $Pin1_{FL}$ complexed to Pintide extrapolated values (*blue-magenta*), $Pin1_{FL}$ complexed to CTD peptide (*cyan*), and $Pin1_{FL}$ complexed to Cdc25 peptide (*white*).

mains are 0.5–1 ns longer than the expected theoretical values. Aggregation may be one explanation for this discrepancy. However, this systematic error is more likely due to an underestimation of complex effects of the flexible linker, which are not adequately captured in the model. Brownian Dynamic simulations[2] may provide a better model for the flexible linker, and future relaxation studies of constructs without the linker will help validate these models.

Comparing the correlation times of Apo-$Pin1_{FL}$ with those of the isolated domains, the τ_c values for $Pin1_{WW}$ and $Pin1_{CAT}$ in Apo-$Pin1_{FL}$ are significantly larger than those for the isolated domains resulting in an inter-domain interaction parameter of 0.47. Thus, on the one hand the linker couples both domains and restricts their flexibility. On the other hand, the difference of about 2 ns between the correlation times of the two domains indicates that Apo-$Pin1_{FL}$ does not tumble as one single rigid body but shows that the two domains tumble independently to a significant extent.

Fig. 4 shows that significantly differing inter-domain interaction parameters account for the experimental data of the three peptides bound to $Pin1_{FL}$, suggesting that distinguishable inter-domain flexibility is induced upon peptide binding. The inter-domain interaction parameter of 0.43 for the Cdc25 peptide bound to $Pin1_{FL}$ is slightly lower than the value for Apo-$Pin1_{FL}$. Therefore, binding of this peptide clearly does not result in any additional flexibility and may even disrupt the interaction among the domains. In contrast to the Cdc25 peptide, the CTD peptide mediates stronger contacts between the two domains as evidenced by the larger *x* value of 0.68. The highest inter-domain interaction parameter of 0.79 is obtained for the Pintide peptide. Thus, this peptide significantly restricts the flexibility of the two domains. An even higher value of $x = 0.85$ is obtained if one extrapolates R_2/R_1 and τ_c values from the actual 85% protein peptide saturation to full saturation. This confirms that Pintide significantly restricts the flexibility of the two domains. Nevertheless, total rigidity ($x = 1$) is not attained, indicating that residual flexibility and possibly hinge bending motions are still present.

In agreement with the chemical shift perturbation, the inter-domain flexibility is reduced in the order Cdc25 < CTD < Pintide. Assuming that peptides bind in a similar orientation as they do in the crystal and NMR structures, the N terminus of the peptides is found to be orientated toward the hydrophobic parts of the inter-domain interaction surface. Hence, hydrophobic residues in the N terminus of the peptide may be decisive for the induction of favorable inter-domain interactions. Indeed, the hydrophobicity of the N terminus increases in the order Cdc25 < CTD < Pintide. However, the size of the peptides decreases in the same order as well. Hence, it cannot be excluded that the two domains form a floppy hydrophobic cleft accommodating molecules only of limited size and that the observed trend is predominantly a steric hindrance effect.

Hydrodynamic Calculations—Hydrodynamic calculations establish the connection between an arbitrarily shaped molecule and its hydrodynamic properties in solution. The program HydroNMR computes NMR relaxation rates R_1, R_2, and {^{1}H}-^{15}N NOEs from a rigid structure (45). Using the atomic coordinate file, a primary hydrodynamic model is built from beads replacing each nonhydrogen atom and having a so-called atomic element radius *a*. In this model the only adjustable parameter is the atomic element radius *a*, with $a = 3.30$ Å being the natural value (46). Larger *a* values indicate aggregation or oligomerization, whereas lower *a* values hint at inter-domain mobility. In our case, the R_2/R_1 ratios of the catalytic

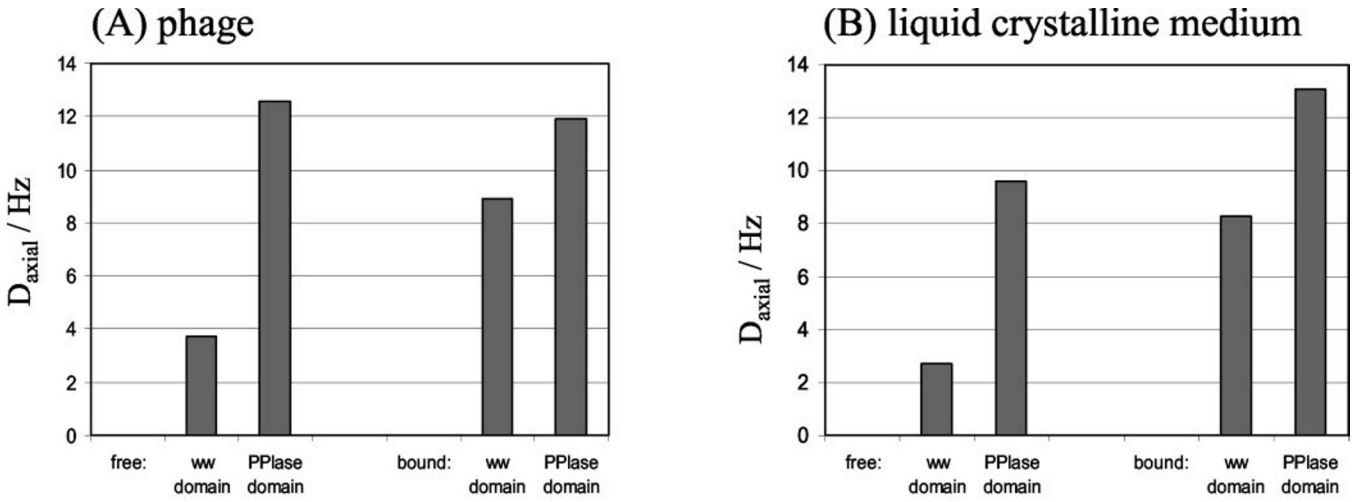

FIG. 5. **Axial component of the alignment tensors (D_{axial}) for phages (*A*) and liquid crystalline medium (*B*).** Values were calculated for Apo-Pin1$_{FL}$ and Pintide bound to Pin1$_{FL}$.

domain and the WW domain differ systematically due to the combination of domain size mismatch and the above discussed domain flexibility. Hence, the a values were derived from fitting to the experimental R_2/R_1 ratios of the catalytic domain only and from using the crystal structure of Ranganathan *et al.* (17) (PDB entry 1PIN). As a result, the calculated R_2/R_1 values agree with the experimental values of the catalytic domain but overestimate the ratios of the WW domain (see Fig. S6, Supplementary Material).

For Pintide bound to Pin1$_{FL}$, the atomic radius parameter a was found to be 3.3 Å. This suggests that both domains interact tightly and tumble almost as a single intact domain. In comparison, the experimental R_2/R_1 of Apo-Pin1$_{FL}$ could only be fitted with an a value of 2.5 Å. For Cdc25 bound to Pin1$_{FL}$ and CTD bound to Pin1$_{FL}$, the a values were calculated to 2.5 and 3.1 Å, respectively. These a values can be interpreted as increasing inter-domain mobility in comparison to Pintide bound to Pin1$_{FL}$. They show the same trend as the inter-domain interaction parameters x.

The degree of anisotropy was calculated from the rotational diffusion tensors computed by HydroNMR and is tabulated in Table SI (Supplementary Material). Evidently, Pin1$_{WW+L}$ ($D_\parallel/D_\perp$ = 1.39) tumbles more anisotropically than Pin1$_{L+CAT}$ ($D_\parallel/D_\perp$ = 1.24). This anisotropy cannot be neglected demonstrating that the assumption of isotropic tumbling is valid only to a first approximation for the discussion above. In comparison to Pin1$_{L+CAT}$, the anisotropy of Pin1$_{FL}$ ($D_\parallel/D_\perp$ = 1.29) does not increase significantly. This does not necessarily indicate that no additional anisotropy is induced by domain contacts, because changes of both the orientation and the size of the diffusion tensors need to be monitored and interpreted.

Residual Dipolar Couplings—The measurement of residual dipolar couplings (RDCs) is a method to derive information about relative domain orientations (*e.g.* Refs. 22, 47, and 48) and motion (22, 23).

Fit of Dipolar Couplings to the Isolated Domains—Relative domain-domain orientations are generally obtained by aligning the tensor orientations of the isolated domains to one orientation for the whole protein. Backbone N-HN heteronuclear RDCs of Apo-Pin1$_{FL}$ and Pintide-bound Pin1$_{FL}$ were measured using two different alignment media, a nonionic liquid crystalline medium (49) and bacteriophages (50).

Our fit of the experimental RDCs to the isolated domains agrees well with the crystallographic data. With respect to Pin1$_{CAT}$, our data fit better to the crystal structure of PDB entry 1PIN (17) than to the crystal structure of PDB entry 1F8A (18). Both structures differ in the region of the phosphate binding loop due to enhanced flexibility and crystal-packing interactions (18). Concerning the flexible loop (residues Ser-16 to Arg-21) of Pin1$_{WW}$, we generally find poor agreement between experimental and predicted data. This loop adopts different conformations in both the x-ray (17, 18) and NMR structures (19, 43) and has been assumed to display a high degree of conformational flexibility.

Size of the Alignment Tensor—In the case of Apo-Pin1$_{FL}$ aligned in both liquid crystalline medium and in phage solution, the distribution of experimental RDCs is much broader for Pin1$_{CAT}$ than for Pin1$_{WW}$, indicating a higher degree of alignment for Pin1$_{CAT}$ than for Pin1$_{WW}$. As seen in Fig. 5 the axial components of the tensors calculated from these values yield a better quantification. In both alignment media, they differ significantly between both domains (D_{axial} (Pin1$_{CAT}$) = 9.6 and D_{axial} (Pin1$_{WW}$) = 2.7 for liquid crystalline medium; D_{axial} (Pin1$_{CAT}$) = 12.6 and D_{axial} (Pin1$_{WW}$) = 3.7 for phages). It is noteworthy that the alignment tensors of Pin1$_{WW}$ are highly imprecise due to the following reasons: (i) Most of the N-H bond vectors in Pin1$_{WW}$ of the available structures have similar orientations. (ii) The small size of Pin1$_{WW}$ results in less RDCs than for Pin1$_{CAT}$. (iii) The available structures differ even in the structurally conserved parts without the flexible loop (residues Ser-16 to Arg-21), thus adding "structural noise." Nevertheless, values found using three different methods are comparable (single value decomposition method (35), the maximum likelihood method (36), and Metropolis Monte Carlo method (37)).

The significant differences of the alignment tensors of the two domains can be interpreted in terms of inter-domain motions (22, 23). Pin1$_{CAT}$ is the larger domain and accounts for 76% of the mass and 71% of the surface area of Pin1$_{FL}$. Assuming that the alignment arises solely from steric factors (33), most of the orientation is expected to be due to interactions between Pin1$_{CAT}$ and the cosolvent. Thus, the greatly diminished alignment tensor of Pin1$_{WW}$ may reflect uncorrelated rotation of this domain with respect to fixed Pin$_{CAT}$.

A partially different picture is found in the case of Pintide-bound Pin1$_{FL}$. For Pin1$_{CAT}$ the dipolar coupling histogram is not changed considerably by the peptide. Also, the resulting principal values and Euler angles of the alignment tensor are similar. Thus, Pin1$_{CAT}$ adopts a similar orientation in comparison to Apo-Pin1$_{FL}$. In contrast, as seen in Fig. 5, both the histogram and the resulting alignment tensor are much larger for peptide-bound Pin1$_{WW}$ than for free Pin1$_{WW}$ (D_{axial}

($Pin1_{CAT}$) = 13.1 and D_{axial} ($Pin1_{WW}$) = 8.3 for liquid crystalline medium; D_{axial} ($Pin1_{CAT}$) = 11.9 and D_{axial} ($Pin1_{WW}$) = 8.9 for phages). As a result, the mobility of $Pin1_{WW}$ with respect to $Pin1_{CAT}$ is reduced significantly upon peptide binding.

Aligning the Two Domains: Structural Implications—A prerequisite for determining the relative orientation of the two domains is that the alignment tensors of both domains are of equal size. Because the alignment tensors differ less in peptide-bound $Pin1_{FL}$ than in Apo-$Pin1_{FL}$ and because the peptide saturation in phages is higher, we concentrated on the alignment of Pintide-bound $Pin1_{FL}$ obtained from the phage solution. Due to the 180° degeneracy of the residual dipolar couplings, the alignment of the two domains normally results in four possible solutions for the average structure with a common tensor orientation (34). In our case, the number of possible structures fulfilling the dipolar coupling data is even higher due to the high rhombicity ($Pin1_{WW}$: 0.57 for PDB entry 1PIN). This leads to a second set of four possible solutions, which are tilted by 90° with respect to the first four possibilities (47), because the *zz*- and *yy*-axes cannot be unambiguously assigned any longer. As a result, one of the eight possible structures agrees with the relative orientation of the crystal structure of PDB entry 1PIN. The other possible solutions can be excluded either because of topological reasons, *i.e.* the distance between the ends of the linker is too large, or because of the disagreement with the observed chemical shift perturbations. This confirms that the relative orientation of the domains in solution is consistent with the x-ray structure.

DISCUSSION

Pin1 uses two domains to facilitate targeting to and isomerization of the pS/T-P binding motif. However, in this process it is unclear whether inter-domain interactions are functionally relevant. Therefore, we investigated the two-domain nature of Pin1 using various NMR methods to address the questions whether the domains interact and, if so, whether different peptides are able to induce inter-domain interactions to a different extent.

Chemical shift perturbation and dynamic studies, including ^{15}N relaxation studies, residual dipolar couplings, and HydroNMR calculation, reveal that the two domains of $Pin1_{FL}$ weakly interact and exhibit significant inter-domain flexibility. The domains interact via hydrophobic contacts between the concave peptide binding surface of the WW domain and the back side (helix α4 and strand β6) of the catalytic domain. Helix α1 does not take part in this interaction. Flexibility of the two domains is markedly modulated by the three peptide substrates used in our study. The inter-domain flexibility is restricted in the order of Cdc25 < CTD < Pintide. The Pintide peptide induces sufficiently strong interactions such that both domains nearly tumble as a single rigid molecule, whereas the Cdc25 peptide induces no additional inter-domain interactions but seems to weaken them. The linker is flexible in solution and is not involved in domain-linker contacts. The interaction site encompasses a hydrophobic cavity comprising the concave peptide-binding surface of the WW domain and the back side (helix α4 and strand β6) of the catalytic domain. For Pintide bound to $Pin1_{FL}$ the crystallographic structure is consistent with residual dipolar coupling data.

Considering that short peptide sequences potentially do not exploit the complete length of the binding site, it remains speculative to what extent our findings are transferable to the full-length substrates. Nevertheless, in the following, two mechanistic models for the interaction of Pin1 with its substrates are discussed in the light of the significant inter-domain flexibility observed.

Wintjens *et al.* (19) and Zhou *et al.* (7) have put forward a sequential model in which phosphorylation of the S/T-P motif is a prerequisite before targeting (via the WW domain) and isomerization (via the catalytic domain) of the same pS/T-P peptide. These two processes can occur subsequently and independently. The sequential order of these events directs the isomerization equilibrium to one specific conformer. Independently of the order, this scenario holds true for one and/or several binding motifs in the substrate. For substrates with repetitive targeting motifs, like Cdc25, an initial binding event may trigger a succession of alternating binding and isomerization steps, each one revealing a further site to be isomerized (1). This hypothesis is consistent with the observation that at high cellular concentrations $Pin1_{CAT}$ is sufficient to carry out the essential function of Pin1 (51). The higher catalytic activity of $Pin1_{FL}$ in comparison to $Pin1_{CAT}$ can be explained by the role of $Pin1_{WW}$ in targeting *trans* pS/T-P motifs and increasing thereby the local concentration of this peptide to be isomerized. In this scenario, inter-domain contacts may serve as an extended recognition surface to control the accessibility of different substrates. However, two functionally separated domains are not mandatory for this sequential model, because the WW domain needs to dissociate in order for the catalytic domain to bind and isomerize the pS/T-P peptide substrate.

The above model can be distinguished from a model in which the WW domain anchors Pin1 to an already phosphorylated pS/T-P motif on another protein, possibly an activated kinase or phosphatase or a protein, which is part of a multienzyme complex involving a kinase or phosphatase. This scenario would enable an efficient "tag and twist" mechanism proposed by Lu *et al.* (5) in which the kinase would "tag" the substrate via phosphorylation and Pin1 would subsequently isomerize or "twist" the pS/T-P imide bond. In this case domain flexibility of Pin1 is crucial if it is to function as a generic "twisting" module working together with a multitude of kinases and phosphatases. A key example for this mechanism could be the C-terminal domain of RNA polymerase II, which exists in a dynamic equilibrium between hypophosphorylated and hyperphosphorylated forms resulting from antagonistic actions of specific kinases and phosphatases. In the context of these kinases and phosphatases, Pin1 is believed to contribute to the regulation of transcription and pre-mRNA maturation by inducing conformational changes after phosphorylation and/or before dephosphorylation of the C terminus (52–54). Similarly, Cdc25C is multiply phosphorylated and activated in part by Cdc2/cyclin B in a positive feedback loop during the G_2/M transition of the cell cycle (1). In this context, $Pin1_{WW}$ may bind to phosphorylated Plk I to provide a complex that first phosphorylates Cdc25C (55) and subsequently activates this substrate by *cis*/*trans* isomerization. Moreover, Pin1 is recruited to the cyclin D1 multienzyme complex (14) and appears to be required for the checkpoint delaying the onset of mitosis in response to incomplete replication (51, 56). We hypothesize that Pin1 can only be recruited and catalytically active in such a multitude of different target protein complexes due to its long flexible linker between the targeting WW domain and the catalytic domain. We believe that Pin1 acts as versatile prolyl *cis*/*trans* isomerization module in conjunction with kinases and phosphatases involved in pS/T-P-mediated signaling, because many of these kinases and phosphatases have pS/T-P motifs themselves.

In conclusion, we have shown that the two domains of Pin1 are loosely connected modules whose mobility is modulated by different peptides. Provided that the substrates can trigger similar modulations in flexibility, variable domain flexibility may enable Pin1 to function in a multitude of different contexts. This near simultaneous execution of phosphorylation and isomerization events offers an intriguing alternative to a sequential and context free targeting and isomerization model.

In the context of protein folding a similar mechanism may also be valid for multidomain PPIases such as FKBP52 (57) or trigger factor (58).

Acknowledgments—We thank Prof. Harald Schwalbe for helpful comments as well as Dr. Michael Baumann and Sarah Mensch for peptide synthesis. Furthermore, we acknowledge Martin Blackledge for making the programs Tensor and Module generally available.

REFERENCES

1. Shaw, P. E. (2002) *EMBO J.* **3,** 521–526
2. Göthel, S. F., and Marahiel, M. A. (1999) *Cell. Mol. Life Sci.* **55,** 423–435
3. Fischer, G., Tradler, T., and Zarnt, T. (1998) *FEBS Lett.* **426,** 17–20
4. Schmid, F. X., Mayr, L. M., Mücke, M., and Schonbrunner, E. R. (1993) *Adv. Protein Chem.* **44,** 25–66
5. Lu, K. P., Liou, Y.-C., and Zhou, X. Z. (2002) *Trends Cell Biol.* **12,** 164–172
6. Sekerina, E., Rahfeld, J. U., Müller, J., Fanghänel, C. R., Fischer, G., and Bayer, P. (2000) *J. Mol. Biol.* **301,** 1003–1017
7. Zhou, X. Z., Lu, P.-J., Wulf, G., and Lu, K. P. (1999) *Cell. Mol. Life Sci.* **56,** 788–806
8. Landrieu, I., Odaert, B., Wieruszeski, J.-M., Drobecq, H., Rousselot-Pailley, P., Inzé, D., and Lippens, G. (2001) *J. Biol. Chem.* **276,** 1434–1438
9. Lu, K.-P., Hanes, S. D., and Hunter, T. (1996) *Nature* **380,** 544–547
10. Ryan, K. M., and Vousden, K. H. (2002) *Nature* **419,** 795–797
11. Zacchi, P., Gostissa, M., Uchida, T., Salvagno, C., Avolio, F., Volinia, S., Ronai, Z., Blandino, G., Schneider, C., and Del Sal, G. (2002) *Nature* **419,** 853–857
12. Zheng, H., Your, H., Zhou, X. Z., Murray, S. A., Uchida, T., Wulf, G., Gu, L., Tang, X., Lu, K. P., and Xiao, Z.-X. J. (2002) *Nature* **419,** 849–852
13. Liou, Y.-C., Ryo, A., Huang, H.-K., Lu, P.-J., Bronson, R., Fujimori, T. U., Hunter, T., and Lu, K. P. (2002) *Proc. Natl. Acad. Sci. U. S. A.* **99,** 1335–1340
14. Ryo, A., Liou, Y.-C., Wulf, G., Nakamura, M., Lee, S. W., and Lu, K. P. (2002) *Mol. Cell. Biol.* **22,** 5281–5295
15. Sudol, M., Sliwa, K., and Russo, T. (2001) *FEBS Lett.* **490,** 190–195
16. Bork, P., and Sudol, M. (1994) *Trends Biochem. Sci.* **19,** 531–533
17. Ranganathan, R., Lu, K. P., Hunter, T., and Noel, J. P. (1997) *Cell* **89,** 875–886
18. Verdecia, M. A., Bowman, M. E., Lu, K. P., Hunter, T., and Noel, J. P. (2000) *Nat. Struct. Biol.* **7,** 639–643
19. Wintjens, R., Wieruszeski, J.-M., Drobecq, H., Rousselot-Pailley, P., Buée, L., Lippens, G., and Landrieu, I. (2001) *J. Biol. Chem.* **276,** 25150–25156
20. Ulmer, T. S., Werner, J. M., and Campbell, I. D. (2002) *Structure* **10,** 901–911
21. Cornilescu, G., Marquardt, J. L., Ottiger, M., and Bax, A. (1998) *J. Am. Chem. Soc.* **120,** 6836–6837
22. Braddock, D. T., Cai, M., Baber, J. L., Huang, Y., and Clore, G. M. (2001) *J. Am. Chem. Soc.* **123,** 8634–8635
23. Tolman, J. R., Al-Hashimi, H. M., Kay, L. E., and Prestegard, J. H. (2001) *J. Am. Chem. Soc.* **123,** 1416–1424
24. Peti, W., Meiler, J., Brüschweiler, R., and Griesinger, C. (2002) *J. Am. Chem. Soc.* **124,** 5822–5833
25. Meiler, J., Prompers, J. J., Peti, W., Griesinger, C., and Brüschweiler, R. (2001) *J. Am. Chem. Soc.* **123,** 6098–6107
26. Kim, S., Cullis, D. N., Feig, L. A., and Baleja, J. D. (2001) *Biochemistry* **40,** 6776–6785
27. Jacobs, D. M., Saxena, K., Grimme, S., Vogtherr, M., Pescatore, B., Langer, T., Elshorst, B., and Fiebig, K. (2002) *J. Biomol. NMR* **23,** 163–164
28. Kay, L. E., Torchia, D. A., and Bax, A. (1989) *Biochemistry* **28,** 8972–8979
29. Grzesiek, S., and Bax, A. (1993) *J. Am. Chem. Soc.* **115,** 12593–12594
30. Dosset, P., Hus, J.-C., Blackledge, M., and Marion, D. (2000) *J. Biomol. NMR* **16,** 23–28
31. Ottiger, M., Delaglio F., and Bax, A. (1998) *J. Magn. Reson.* **131,** 373–378
32. Meissner, A., Duus, J. Ø., and Sørensen, O. W. (1997) *J. Biomol. NMR* **10,** 89–94
33. Zweckstetter, M., and Bax, A. (2000) *J. Am. Chem. Soc.* **122,** 3791–3792
34. Al-Hashimi, H. M., Valafar, H., Terrell, M., Zartler, E. R., Eidsness, M. K., and Prestegard, J. H. (2000) *J. Magn. Reson.* **143,** 402–406
35. Losonczi, J. A., Andrec, M., Fischer, M. W. F., and Prestegard, J. H. (1999) *J. Magn. Reson.* **138,** 334–342
36. Warren, J. J., and Moore, P. B. (2001) *J. Magn. Reson.* **149,** 271–275
37. Dosset, P., Hus, J.-C., Marion, D., and Blackledge, M. (2001) *J. Biomol. NMR* **20,** 223–231
38. Yaffe, M. B., Schutkowski, M., Shen, M., Zhou, X. Z., Stukenberg, P. T., Rahfeld, J.-U., Xu, J., Kuang, J., Kirschner, M. W., Fischer, G., Cantley, L. C., and Lu, K. P (1997) *Science* **278,** 1957–1960
39. Landrieu, I., Wieruszeski, J.-M., Wintjens, R., Inzé, D., and Lippens, G. (2002) *J. Mol. Biol.* **320,** 321–332
40. Bayer, E., Goettsch, S., Mueller, J. W., Griewel, B., Guiberman, E., Mayr, L. M., and Bayer, P. (April 29, 2003) *J Biol. Chem.* **278,** 26183–26193
41. Zhang, Y., Füssel, S., Reimer, U., Schutkowski, M., and Fischer, G. (2002) *Biochemistry* **41,** 11868–11877
42. Schutkowski, M., Bernhardt, A., Zhou, X. Z., Shen, M., Reimer, U., Rahfeld, J.-U., Lu, K. P., and Fischer, G. (1998) *Biochemistry* **37,** 5566–5575
43. Kowalski, J. A., Liu, K., and Kelly, J. W. (2002) *Biopolymer* **63,** 111–121
44. Peng, J. W., and Wagner, G. (1994) *Methods Enzymol.* **239,** 536–596
45. Garcia de la Torre, J., Huertas, M. L., and Carrasco, B. (2000) *J. Magn. Reson.* **147,** 138–147
46. Bernadó, P., García de la Torre, J., and Pons, M. (2002) *J. Biomol. NMR* **23,** 139–150
47. Fischer, M. W. F., Losonczi, J. A., Weaver, J. L., and Prestegard, J. H. (1999) *Biochemistry* **38,** 9013–9022
48. Braddock, D. T., Louis, J. M., Baber, J. L., Levens, D., and Clore, G. M. (2002) *Nature* **415,** 1051–1056
49. Rückert, M., and Otting, G. (2000) *J. Am. Chem. Soc.* **122,** 7793–7797
50. Hansen, M. R., Mueller, L., and Pardi, A. (1998) *Nat. Struct. Biol.* **5,** 1065–1074
51. Zhou, X. Z., Kops, O., Werner, A., Lu, P.-J., Shen, M., Stoller, G., Küllertz, G., Stark, M., Fischer, G., and Lu, K. P. (2000) *Mol. Cell* **6,** 873–883
52. Lavoie, S. B., Albert, A. L., Handa, H., Vincent, M., and Bensaude, O. (2001) *J. Mol. Biol.* **312,** 675–685
53. Kops, O., Zhou, X. Z., and Lu, K. P. (2002) *FEBS Lett.* **513,** 305–311
54. Hani, J., Schelbert, B., Bernhardt, A., Domdey, H., Fischer, G., Wiebauer, K., and Rahfeld, J.-U. (1999) *J. Biol. Chem.* **274,** 108–116
55. Stukenberg, P. T., and Kischner, M. W. (2001) *Mol. Cell* **7,** 1071–1083
56. Winkler, K. E., Swenson, K. I., Kornbluth, S., and Means, A. R. (2000) *Science* **287,** 1644–1647
57. Galat, A. (2000) *Eur. J. Biochem.* **267,** 4945–4959
58. Zarnt, T., Tradler, T., Stoller, G., Scholz, C., Schmid, F. X., and Fischer, G. (1997) *J. Mol. Biol.* **271,** 827–837